International Journal of Automotive Technology
https://doi.org/10.1007/s12239-024-00134-3

Stabilizing Electric Vehicle Systems Using Proximal Policy-Based Self-structuring Control

Juntao Zhuang[1] · Chengwei Wang[2] · Qiong Cheng[1] · Ying Dai[6] · Ebrahim Ghaderpour[4] · Ardashir Mohammadzadeh[3,5]

Received: 27 March 2024 / Revised: 30 April 2024 / Accepted: 8 July 2024

Abstract
An active disturbance rejection control (ADRC) has been developed for stabilizing electric vehicle (EV) systems without the need for model identification. The proximal policy optimization (PPO) algorithm, along with actor and critic neural networks, has been used to fine-tune the adjustable parameters of the ADRC controller to achieve optimal performance in a specific case study. The architecture of PPO implements separate neural networks and ameliorates the PPO adaptability to handle continuous action spaces. By maximizing a reward function based on system output, the PPO agent optimally tunes the gains to reduce undesired speed fluctuations of EVs and improve system stability. Performance evaluation under the new European driving cycle and federal test procedure has been conducted to examine the feasibility of the suggested controller. The disturbance rejection capability of the ADRC controller designed by the PPO algorithm has been tested and compared with prevalent control methodologies. Moreover, real-time examinations of the dynamic behavior of EV systems have been made to identify the capability of the suggested controller in real-world hardware. The results show that the suggested controller outperforms other designed controllers in terms of transient behavior and numerical performance metrics.

Keywords Electric vehicles (EVs) · Active disturbance rejection control (ADRC) · Proximal policy optimization (PPO) · New European driving cycle (NEDC) · Federal test procedure (FTP-75)

1 Introduction

Electric vehicles (EVs) have recently emerged as a prominent solution to face environmental problems and the shortage of conventional fossil fuel sources (Pazouki & Olamaei, 2019; Mamo, Gopal, and Yoseph 2024; Hasan et al., 2024). The EVs have the potential to tackle these problems and many more benefits over the traditional internal combustion engine (ICE) vehicle like quiet operation, low fueling costs, and high efficiency. Their popularity in the transformation industry has been further fueled by advances in battery technologies, making EVs more practical for a wide reasonable range of consumers. With increased research and development in the EV sector, it is anticipated that these technologies will soon experience a greater transition toward sustainability (Alrubaie et al., 2023; Bozhi et al., 2023; Bristi et al., 2023).

The battery pack, electric motor, power electronic components, charging ports, power train, and control mechanism are the main elements of an electric vehicle system. Among the various components, the controller in EV plays a critical role in managing and optimizing various aspects of the vehicle's performance (Djouahi et al., 2023; Hwang et al., 2024). However, the regulation of EV output is a challenging task, because these technologies have a time-variant nature (e.g., parametric variation of system dynamic, change in the

✉ Ebrahim Ghaderpour
ebrahim.ghaderpour@uniroma1.it

[1] Geely Automotive Institute, Hangzhou Vocational & Technical College, No.68 Xueyuanjie, Xiasha, Hangzhou 310000, Zhejiang, China

[2] Seres Automotive Co., Ltd, Chongqing 404100, China

[3] Multidisciplinary Center for Infrastructure Engineering, Shenyang University of Technology, No.111, Shenliao West Road, Shenyang 110870, China

[4] Department of Earth Sciences, Sapienza University of Rome, Piazzale Aldo-Moro, 5, 00185 Rome, Italy

[5] Department of Electrical Engineering, University of Bonab, Bonab, Iran

[6] College of Architecture and Civil Engineering, Shenyang University of Technology, Shenyang, China

Published online: 09 August 2024

road condition, etc.) (George et al., 2021; Liu et al., 2022). One of the challenges of current EVs is the limited driving distance per battery charge, which restricts their applicability. Therefore, apart from regulating the performance of EVs, the energy stored in the battery system is also managed during its operation. The ability to optimally utilize and store the power during driving is essential to tackle the limitations and improve the practicality of EVs (Khooban, Niknam, and Sha-Sadeghi 2016b; Xiao et al., 2023; Zhang et al., 2023).

Numerous control algorithms have been developed to regulate the output power of EVs in various industry and transportation applications, ranging from linear controllers such as linear matrix inequality (LMI) (Cheng et al., 2020), linear quadratic integral (LQI) (Ristiana et al., 2019), H-infinity control (Cheng et al., 2020) to non-linear controller like sliding mode control (SMC) (Deng et al., 2022; Subroto et al., 2020), fractional order (Ahmed et al., 2021), fuzzy logic (Khooban, Niknam, and Sha-Sadeghi 2016b), and backstepping (Pang et al., 2021). For instance, (George et al., 2021) developed a fractional-order version of fuzzy logic for the stabilization of EV systems under the European driving cycle (NEDC) test. However, the suggested controller by (George et al., 2021) suffers a lack of learning and adaptation capability which degrades its performance against external disturbance. A general type-2 fuzzy logic based on SMC was proposed by (Khooban et al., 2016a, 2016b) to solve the problem of EV systems under un-modeled dynamics and external disturbances. The proposed controller by (Khooban et al., 2016a, 2016b) needs to mathematical modelling of EV system which necessitates high complexity during control design stage. (Haddoun et al., 2008) utilized the recurrent neural network (RNN) estimator to improve the performance of the EV system under the urban ECE-15 cycle. Despite a robust speed estimation performance obtained by the proposed scheme, the need to a large dataset for training the neural network imposes sever challenges associated with that the application. (Zhu et al., 2016) developed a new slip control mechanism equipped with nonlinear model predictive control for safety objective of EV system subjected to system constraints. The performance of the controller may be sensitive to the selection of dynamic parameters and cost function weights, making it challenging to find an optimal configuration.

Since the model-based controllers are often developed based on mathematical modeling, any uncertainties and un-modeled dynamics in the EV system degrade their performance. Active disturbance rejection control (ADRC) (Meng, Liu, and Wang 2019; Yang et al., 2022) has emerged as an advanced control strategy that can estimate and compensate the disturbances in a real-time framework. In the structure of the ADRC controller, an extended state observer (ESO) is adopted to estimate the unpredictable disturbances and unknown dynamics of a controlled plant and compensate for their effect in the feedback path. This data-driven control scheme is well known due to its straightforward structure, high accuracy, and quick response, besides its capability to tackle uncertainties regardless of the system dynamics. The potential of the ADRC controller has been proved in many applications, such as wind turbines (Wu et al., 2020; Xia et al., 2013), unmanned aerial vehicles (UAVs) (Niu, Xiong, and Zhao 2016), humanoid robots (Li, Luo, and Dou 2022), power interface systems (Tao et al., 2021), and magnet synchronous motors (Zhao & Dong, 2019).

The ADRC controller has many control parameters that should be appropriately regulated to achieve the desired performance from the control engineering point of view. Adjusting these coefficients is a challenging task, especially in dealing with sophisticated and partly known systems. To address this issue, many efforts have been made by contemporary researchers to tune the gains of ADRC controllers such as fuzzy logic (Li et al., 2019; Tao et al., 2018), meta-heuristic algorithms (Yang et al., 2022; Li, Shi, and Zhang 2021), gain scheduling (Wu et al., 2019), etc. (Li et al., 2019) used fuzzy logic to tune the gains embedded in the structure of the ADRC controller to enhance the adaptability of unmanned aerial vehicles to the marine environment. However, the need to set the rule base of fuzzy sets is a difficult task that necessitates expert knowledge or employing tools for rule optimization. (Kang et al., 2019) introduced a hybrid scheme based on the principle of artificial fish swarm and particle swarm algorithms to tune the decisive parameters of the ADRC controller. The proposed scheme by (Kang et al., 2019) suffers the complexity of a combined intelligent algorithm which demands accurate parameter tuning and high computational time. (Wu et al., 2019), designed a gain scheduling technique based on ADRC to tackle the challenges of safe operation and regulation of integrated renewable energy systems. However, the primary limitation of the gain scheduling scheme lies in the complexity associated with adjusting the scheduling parameters to achieve optimal response in the face of changing operating conditions. Generally, the aforesaid optimization methodologies suffer the lack of training, limited exploration and sensitivity to initial conditions which limit their application scope in complex problems.

Reinforcement Learning (RL) is known as one of the most important branches of artificial intelligence (AI) (Bhatti et al., 2021, 2023) which can optimize the control techniques through interacting the agent with the unknown environment (Hu et al., 2019; Qiu et al., 2023; Wang et al. 2023; Chen et al., 2023). The RL agent updates the parameters of the controller by maximizing a reward function where the terms of states and value function are updated during the execution of action signals. Among

various types of RL algorithms, the application of SARSA (State-Action-Reward-State-Action) and Q-learning has drawn significant attention in various fields of control engineering (Dabbaghjamanesh et al., 2020; Ozcelik et al., 2022). Despite the successful performance of these algorithms in many applications, the need for Q-Table to store the learned Q-values leads to large computational requirements. The necessity to create and update the Q-Table becomes impractical in high-dimensional continuous problems. Apart from this, the sensitivity to hyperparameters and convergence to suboptimal policies limit their applications. More recently, an advanced version of the deep RL algorithm, called proximal policy optimization (PPO) (Zhang et al., 2021), was introduced that addresses the challenges of Q-Table-based algorithms. This algorithm has the benefit of being an on-policy scheme using a clipped surrogate objective, which makes it more suitable for exploring the optimal solutions for both discrete and continuous action environments.

Despite the rich body of literature in the context of EVs, there are some challenges that limit the feasibility of deterministic robust controllers. Inherent uncertainties and complexities of EVs make it difficult to obtain a mathematical model to capture all the aspects accurate model of system dynamics. Under this circumstance, deploying robust controllers for the speed regulation of EVs is not reasonable due to practical considerations. To address this, the current paper aims to develop an intelligent data-driven controller to address the stabilization problem of EV speed in the presence of un-modeled dynamics and external disturbances. For this purpose, the ADRC controller has been adaptively adjusted by the PPO algorithm to improve the performance of EV systems. The proposed tuner mechanism can obtain the control requirements and has the potential to tackle the uncertainties. The main contributions are given as follows.

(1) The problem of EV is formulated to study the challenges of speed control to compensate for the nonlinear dynamics and uncertainties.
(2) A data-driven controller based on the ADRC scheme has been designed to stabilize the speed output of electric vehicle systems. In this context, ADRC is developed without the need for accurate knowledge of the model identification, which simplifies the control strategy.
(3) The coefficients embedded in the structure of the established ADRC controller have been adjusted by the PPO algorithm. This involves defining a reward function according to the EV output which provides the capability to tune the control gains through interacting the PPO agent with the environment.
(4) The training ability of the PPO agent allows the ADRC to adapt according to the characteristics of the EV system and optimize the performance without relying on system dynamics.

Many typical scenarios, especially under the NEDC test and FTP-75, are considered to assess and demonstrate the usefulness of the suggested data-driven controller (realized by the PPO algorithm) in stabilizing EV speed. Since the proposed control framework is designed in a data-driven manner, it can be adopted for wide reasonable electric vehicle systems. The current work is organized as follows: The dynamic modeling of the EV system is formulated in Sect. 2. In Sect. 3, the principle of ADRC control for the stabilization of the case study is elaborated, and the PPO algorithm for the optimal design of the control gains is presented. In Sect. 4, simulation examinations of typical scenarios of EV systems are carried out, followed by the justification of using the proposed framework, as presented in Sect. 5. The main outcomes of this research work are concluded in Sect. 6.

2 Dynamic Modelling of EV System

The electric vehicle (EV) is a complex system with various components that work in a union to offer efficient and sustainable transportation. The main elements of an EV comprise of control unit, battery system, and electric motors, all the components are connected to the vehicle by a transmission system. Various generation units, such as fuel cells (FC), photovoltaic (PV), and battery units can be responsible for supplying the EV systems (Khooban, Niknam, and

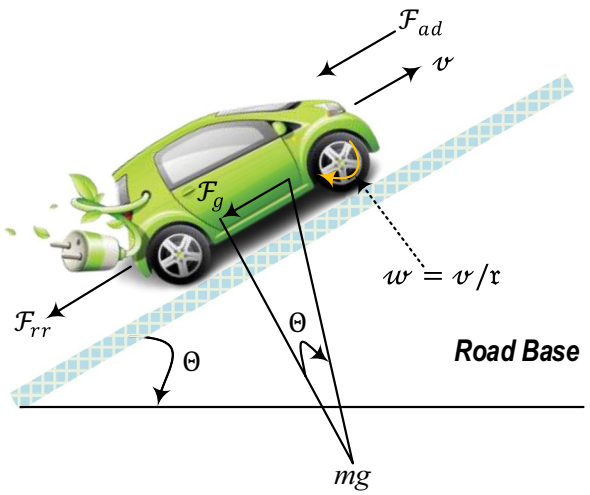

Fig. 1 The illustration of applying various forces to EV on a road

Sha-Sadeghi 2016b; Das et al., 2022). The dynamics of the EV system can be elaborated into two separate parts: vehicle dynamics and motor dynamics. Figure 1 illustrates the schematic of various forces which are applied to the EV system on the road.

The road loads encompass several key elements, namely, the resistance posed by tire rolling, the gravitational force due to the Earth's pull, the aerodynamic drag force (ADF) caused by air resistance, and the force incurred when ascending hills (hill-climbing force or HCF). The total traction force ($\mathcal{F}_{Tot}$) of vehicle dynamic can be elaborated by considering all the forces including rolling friction ($\mathcal{F}_{rr}$), gravity of earth ($\mathcal{F}_{ge}$), aerodynamic drag ($\mathcal{F}_{ad}$), vehicle acceleration ($\mathcal{F}_{a}$), given as (Khooban, Niknam, and Sha-Sadeghi 2016b; George et al., 2021):

$$\mathcal{F}_{Tot} = \mathcal{F}_{rr} + \mathcal{F}_{ge} + \mathcal{F}_{ad} + \mathcal{F}_{a} \tag{1}$$

$$\mathcal{F}_{Tot} = \psi_{rr} mg + 0.5\rho A C_d v^2 + mg\sin\Theta + m(dv/dt) \tag{2}$$

where v and A denote the driving velocity and the frontal area, respectively; m is the vehicle's mass; the rolling resistance is denoted by ψ_{rr}; the air density is denoted by ρ; g is the gravity acceleration; Θ is the hill-climbing angle; C_d is the drag factor. Likewise, in Eq. (2), the term of '$\psi_{rr}mg$' simplifies the force of $\mathcal{F}_{rr}$; '$0.5\rho AC_d v^2$' is related to the force of ADF; '$mgsin\Theta$' represents the force of HCF; 'dv/dt' denotes the acceleration force. In the EV system, a torque $\mathcal{T}_L$ will be produced by $\mathcal{F}_{Tot}$ to drive the motor, given by:

$$\mathcal{T}_L = \mathcal{F}_{Tot} \times \left(\frac{r}{\mathcal{G}}\right) \tag{3}$$

where r denotes the tire radius; $\mathcal{G}$ denotes the gearing ratio. According to (George et al., 2021), the model of the electric motor is defined by non-linear relations, which are defined by:

$$\frac{di}{dt} = \frac{1}{\left(\mathcal{L}_a + \mathcal{L}_{field}\right)}\left\{\mathcal{V} - \left(R_a + R_f\right)i - \mathcal{L}_{af} i.w\right\} \tag{4}$$

$$\frac{dw}{dt} = \frac{1}{J}\left\{\mathcal{L}_{af} i^2 - \mathcal{T}_L - Bw\right\} \tag{5}$$

In Eqs. (4) and (5), the armature current is denoted by i; the angular speed is represented by w; the winding resistance is denoted by R_f; the armature resistance is denoted by R_a; $\mathcal{L}_a$ is the armature inductance; $\mathcal{L}_{field}$ is the winding inductance; B is the viscous factor; J is the inertia; v is the input voltage; $\mathcal{L}_{af}$ is mutual inductance (George et al., 2021; Veysi et al., 2020). Therefore, the driving velocity of the EV system given as $v = w \times \left(\frac{r}{\mathcal{G}}\right)$. By integrating the electrical and motor models, the overall model of EV is defined as follows (Veysi et al., 2020).

$$\frac{di}{dt} = \frac{1}{\left(\mathcal{L}_a + \mathcal{L}_{field}\right)}\left(\mathcal{V} - \left(R_a + R_f\right)i - \mathcal{L}_{af} i.w\right) \tag{6}$$

$$\frac{dw}{dt} = \frac{1}{\left(J + m(\mathfrak{r}/\mathcal{G})^2\right)}\left\{\mathcal{L}_{af} i^2 - Bw - \frac{\mathfrak{r}}{\mathcal{G}}\left(\psi_{rr} mg + \frac{1}{2}\rho A C_d v^2 + mg\sin\Theta\right)\right\} \tag{7}$$

Based on the above relations, the block diagram schematic of the EV system is drawn as shown in Fig. 2.

The state space form of Eqs. (6) and (7) is given as:

$$\dot{X} = f(X) + g(X)u \tag{8}$$

$$X = \begin{bmatrix} x_1 \\ x_2 \end{bmatrix} = \begin{bmatrix} i \\ \omega \end{bmatrix} \tag{9}$$

The fucntions of $f(X)$ and $g(X)$ are defined as eqs. (10) and (11).

The main goal of the EV problem is to the speed output (w) track its reference (w_{ref}). Unlike many other practical system applications, electric vehicle units are characterized to operate at a wide range of speeds,

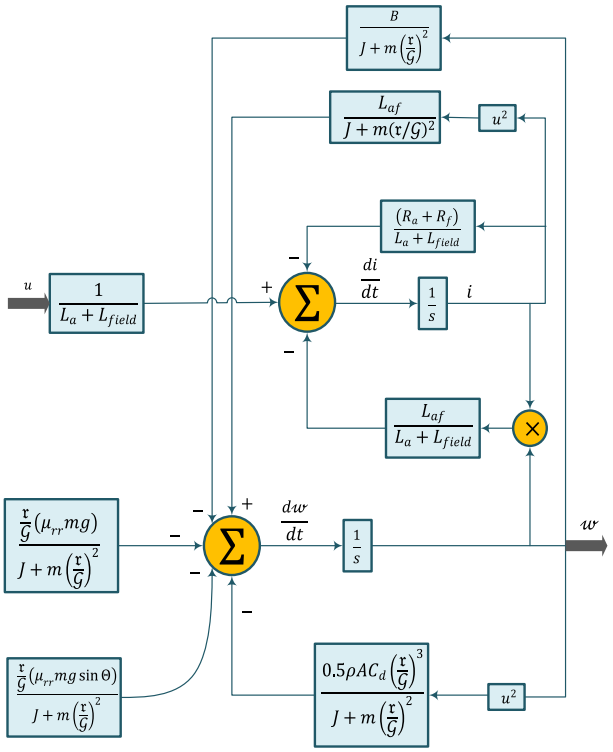

Fig. 2 The overall structure of the EV system

ranging from zero to maximum speed. Consequently, the deployment of controllers for optimal stabilization of EVs necessitates non-linear control methodologies.

3 Design of Adrc Controller Based on Ppo Tuner Mechanism

3.1 Active Disturbance Rejection Controller

Generally, a system with the output $\mathcal{O}$ and input $u(t)$ can be defined by the first order representation, given as:

$$\mathcal{O}^{(n)}(t) = bu(t) + g\Big(t, \mathcal{O}, \ddot{\mathcal{O}}, \ldots d, \mu\Big)\Big\} \tag{10}$$

where b is the input factor; g denotes the synthesis function; $\ddot{\mathcal{O}}$ denotes the high order of $\mathcal{O}$; d the external disturbances; μ is uncertainties. By defining $f(t) = g(t) + \Big(b - \widehat{b}\Big)u(t)$, where $\widehat{b}$ denotes estimation of b, Eq. (12) can be written as:

$$\mathcal{O}^{(n)}(t) = \widehat{b}u(t) + f(\bullet) \tag{11}$$

where n denotes the order of $\mathcal{O}$; $f(\bullet)$ denotes the total disturbance. The tracking differentiator (TD) is the first part of ADRC, employed for tracking the system behavior. The main role of TD is to differentiate the tracking error, i.e., the difference between the actual output with the reference signal,

given as:

$$\begin{aligned} fh &= fhan\Big(z_{11}(t) - \mathcal{O}^*(t), z_{12}(t), T, h\Big) \\ z_{11}(t+1) &= z_{11}(t) + h * z_{12}(t) \\ z_{12}(t+1) &= z_{12}(t) + h * fh \end{aligned} \tag{12}$$

where the outputs of the TD are expressed by $z_{11}(t)$ and $z_{12}(t)$; h denotes the sampling period; T is the tracking variable; $\mathcal{O}^*(t)$ denotes the reference signal. Likewise, $fhan(\bullet)$ is an integrated function with the following definitions:

$$fhan(\bullet) = \begin{cases} -Tsign(\sigma), |\sigma| > \xi \\ -T\frac{\sigma}{\xi}, |\sigma| \le \xi \end{cases} \tag{13}$$

where

$$f(X) = \begin{bmatrix} -\frac{R_a+R_f}{\mathcal{L}_a+\mathcal{L}_{field}}x_1 - \frac{\mathcal{L}_{af}}{\mathcal{L}_a+\mathcal{L}_{field}}x_1.x_2\Big(\frac{1}{J+m(\mathfrak{r}/\mathcal{G})^2}\Big)\mathcal{L}_{af}x_1^2 \\ -Bx_2 - \mathfrak{r}/\mathcal{G}\Big(\mu_{rr}mg + \frac{1}{2}\rho AC_d(\mathfrak{r}/\mathcal{G})^2x_2^2 + mgsin\Theta\Big) \end{bmatrix} \tag{14}$$

$$g(x) = \begin{bmatrix} \Big(\frac{1}{\mathcal{L}_a+\mathcal{L}_{field}}\Big) \\ 0 \end{bmatrix} \tag{15}$$

$$\begin{aligned} \xi = T.h, \xi_0 = \xi.h \\ O = z_{11} + hz_{12} \\ \sigma_0 = \sqrt{\xi^2 + 8.T|y|} \\ \sigma = \begin{cases} z_{12} + \frac{\sigma_0-\xi}{2}sign(y), |y| > \xi_0 \\ z_{12} + \frac{\mathcal{O}}{h}, |y| \le \xi_0 \end{cases} \end{aligned} \tag{16}$$

In the ADRC framework, both the un-modeled dynamics and parameter perturbations in the system are regarded as the total disturbance which should be estimated by an observer. To do this, an extended state observer (ESO) is embedded in the feedback path of the control loop to estimate all the uncertainties. A three-order form of ESO is elaborated by:

$$\begin{aligned} e(t) &= z_{21}(t) - \mathcal{O}(t) \\ z_{21}(t+1) &= z_{21}(t) + h\Big(Z_{22}(t) - \beta_{01}e(t)\Big) \\ z_{22}(t+1) &= z_{22}(t) + \\ & h\Big(z_{23}(t) - \beta_{02}fal\Big(e(t), \tfrac{1}{2}, \delta\Big) + b_0u\Big) \\ z_{23}(t+1) &= z_{23}(t) - h\beta_{03}fal\Big(\varepsilon(t), \tfrac{1}{4}, \delta\Big) \end{aligned} \tag{17}$$

where $e(t)$ is the error signal of the ESO; z_{21}, z_{22}, z_{23} are the estimated values of the observer; β_{01}, β_{02} and β_{03} are the tunable parameters of the observer; δ is a filtering variable. Moreover, the term $fal(\bullet)$ is a nonlinear function, which is defined by:

$$fal(e, \alpha, \delta) = \begin{cases} |e|^{\alpha}sign(e), |e| > \delta \\ e/\delta^{1-\alpha}, |e| \le \delta \end{cases} \tag{18}$$

In addition, a nonlinear state error feedback (NLSEF) is also incorporated in the ADRC controller to mitigate and reduce the effect of disturbances using the differential signal produced by TD (z_{11}, z_{12}) and the estimated values (z_{21}, z_{22}) obtained by ESO. The mathematical expression of NLSEF is given in the following form.

$$\begin{cases} e_1 = z_{11} - z_{21} \\ e_2 = z_{12} - z_{22} \\ u_0 = \beta_1fal\big(e_1, \alpha_1, \delta\big) + \beta_2fal\big(e_2, \alpha_2, \delta\big) \end{cases} \tag{19}$$

where the control gains of NLSEF are denoted by β_1 and β_2. Using the estimated states obtained by ESO, the control law for compensating the disturbances is defined by:

$$u(t) = u_0 - z_{23}/b_0 \tag{20}$$

The schematic of the structured ADRC scheme for speed stabilization of the EV system is illustrated in Fig. 3.

Remark 1: The ADRC controller is designed as a data-driven scheme that can regulate the speed of the EV system without the need to model identification. While the model-based schemes should be designed according to the system

model, ADRC can stabilize the system output by the input/output data.

3.2 Proximal Policy Optimization Algorithm

Reinforcement Learning (RL) refers to the way that an agent learns from experiences by taking return (or reward) signals from the environment (system). The mathematical framework to model the RL algorithm is recognized as Markov Decision Process (MDP). An overall representation of RL-based algorithms for the stabilization of EV systems is illustrated in Fig. 4. According to Fig. 4, the agent or controller applies the control actions to the EV system to obtain the desired goal. As a result, the new state and reward signal is received by the agent.

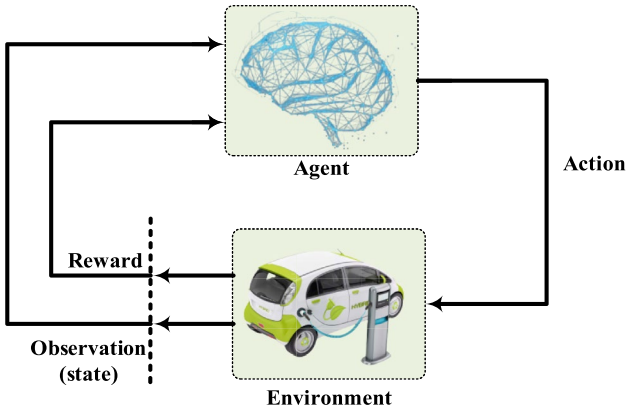

Fig. 4 Illustration of RL algorithm applied to EV system

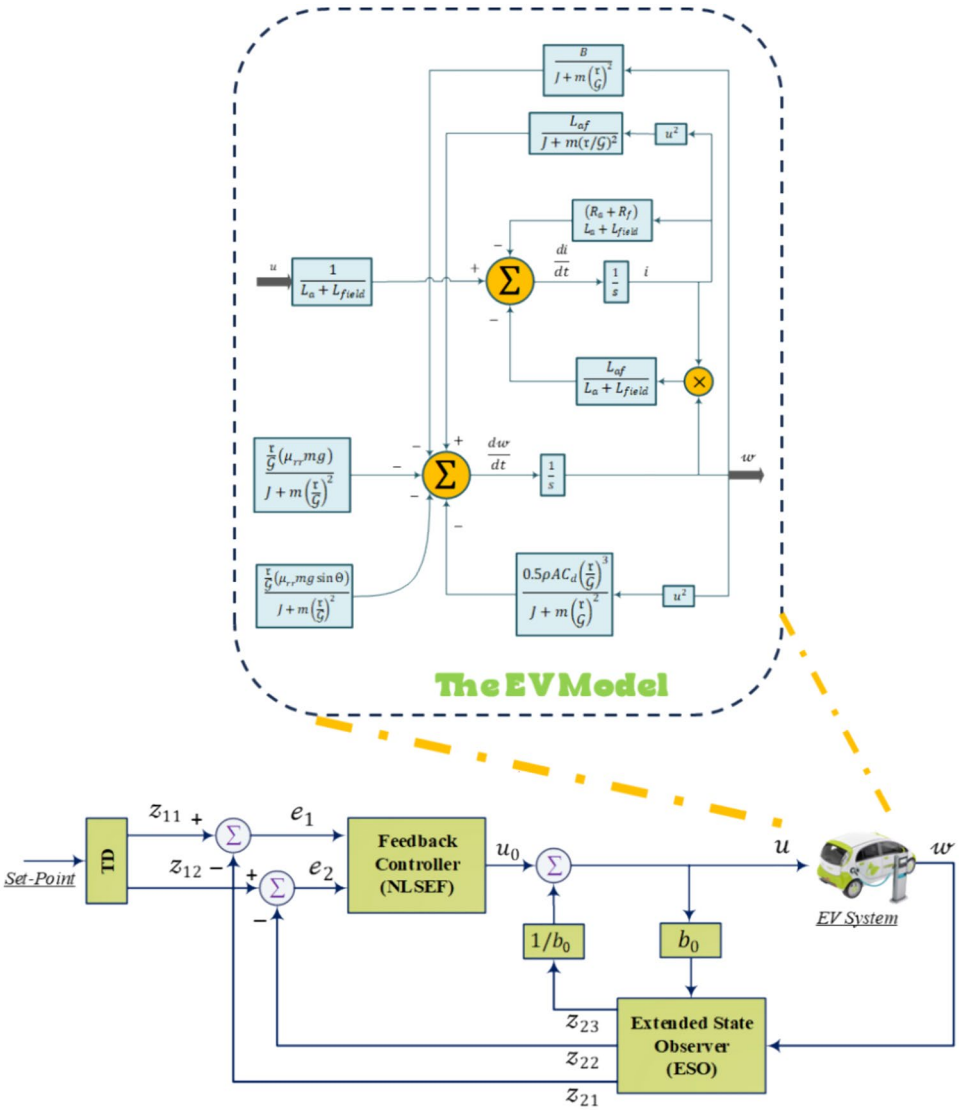

Fig. 3 Schematic of ADRC controller with the components of TD, ESO, and NLSEF

The PPO is a policy-gradient (PG) scheme based on the RL algorithm that is designed to maximize the policy of an agent. The main goal of the PG scheme is to address the problem of policy optimization in such a way that balances exploration and exploitation. In the native algorithm, the policy net π with the weight of θ takes the state $\int$ as the input signal (observation) and produces an action $\dashv$. In the context of continuous action space, the policy net's responsibility is to generate key statistical parameters of a probability distribution, especially the means and variances of a Gaussian distribution, which are adopted to generate control actions. To ameliorate the exploration, the PPO agent generates actions using a random sample of this distribution during the training process. Once the training procedure is completed, the mean of the distribution is chosen as the action.

A typical architecture of PPO integrates the actor and critic nets using the PG scheme. The role of the actor net is to select actions by adjusting the weight parameters of policy while the critic net is responsible for improving the actor net by calculating the desirability of taken actions in specific states. In the PG, the objective function with the weight of θ is updated by:

$$\mathcal{L}(\theta) = \hat{\mathrm{E}}_t\left[\log \pi_\theta\left(a_t|s_t\right)\mathcal{A}_t\left(a_t|s_t\right)\right] \tag{21}$$

where $\hat{\mathbb{E}}_t$ denotes the expected value with respect to step time t, $\mathcal{A}_t\left(a_t|s_t\right)$ denotes the superiority function which is defined by the following expression.

$$\mathcal{A}_t(s,a) = \mathcal{Q}_t\left(s_t,a_t\right) - V_t\left(s_t\right) \tag{22}$$

The updating of θ is by the PG algorithm is given as:

$$\theta_{t+1} = \theta_t + a\nabla_\theta \mathcal{L}\left(\theta_t\right) \tag{23}$$

Since the PG algorithm faces the challenges of choosing the proper step size, the PPO addresses this issue by utilizing a modified objective function:

$$\mathcal{L}^{CPI}(\theta) = \hat{\mathrm{E}}_t\left[\frac{\pi_\theta\left(a_t|s_t\right)}{\pi_{\theta_{old}}\left(a_t|s_t\right)}\mathcal{A}_t\right] = \hat{\mathrm{E}}_t\left[r_t(\theta)\mathcal{A}_t\right] \tag{24}$$

The Kullback–Leibler (KL) divergence is often adopted to stabilize the training process. In the PPO algorithm, a limitation is introduced on the KL between new policies $\left(\pi_\theta\left(a_t|s_t\right)\right)$ and old policy $\left(\pi_{\theta_{old}}\left(a_t|s_t\right)\right)$. The actor and critic nets are aimed to maximize the surrogate function, expressed by:

$$\mathcal{L}^{clip}(\theta) = \hat{\mathrm{E}}_t\left[\min\left(r_t(\theta)\hat{A}_t.clip\left(r_t(\theta),1-\varepsilon,1+\varepsilon\right)\right)\hat{A}_t\right] \tag{25}$$

where $\widehat{A}$ is advantage function A; ε denotes a truncation constant. The ratio of old and new schemes is defined by:

$$r_t(\theta) = \frac{\pi_\theta\left(a_t,s_t\right)}{\pi_{\theta_{old}}\left(a_t,s_t\right)} \tag{26}$$

The procedure steps and architecture of PPO with actor and critic framework are demonstrated in Algorithm 1 and Fig. 5.

Initialize the policy parameters

for i=0, 1, 2,… **do**

Collect trajectories by applying the policy π_θ to the environment.

Calculate the return signals r_t under the under-taken action.

Obtain the advantage estimates $\hat{A}_t$ using the advantage estimation scheme

Compute policy update:

$$\theta_{t+1} = arg\max_\theta \mathcal{L}_{\theta_k}^{CPI}(\theta)$$

by taking k step of mini-batch (via Adam optimizer),

$$\mathcal{L}_{\substack{\theta_{t+1}\\ k}}^{CPI}(\theta) = \hat{\mathbb{E}}_t\left[\sum_{t=0}^{M} min\left(r_t(\theta)\hat{A}_t.clip\left(r_t(\theta),1-\varepsilon,1+\varepsilon\right)\right)\hat{A}_t\right]$$

end for

Algorithm 1

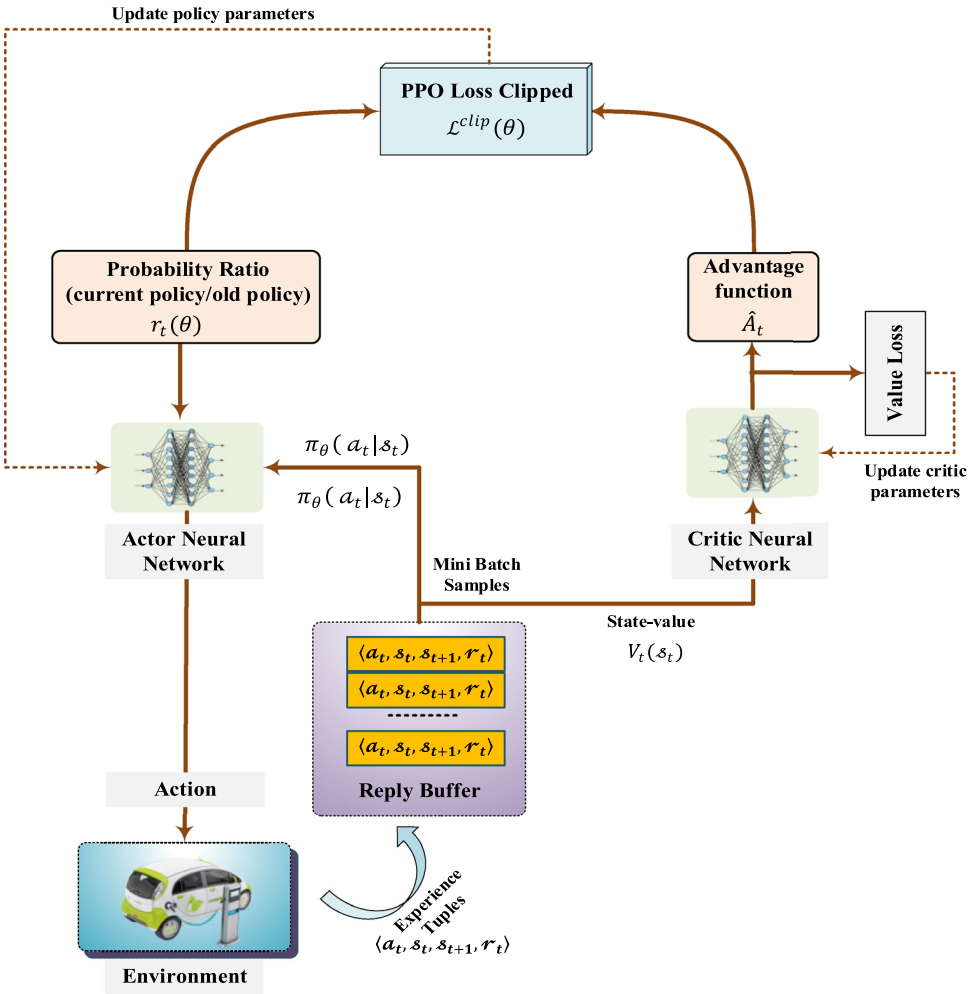

Fig. 5 The architecture of the PPO Algorithm applied to the EV system

The computational resources required to deploy the PPO algorithm depend on many factors which vary according to the complexity of the problem and the desired level of real-time operation. The size of neural nets, real-time constraints, tuning of hyper-parameters, and optimization methodologies are the main factors that play a crucial role in determining the computational demand of PPO in real-time applications.

Remark 2: Note that control actions of the PPO algorithm are bounded where the PPO mechanism updates its control policy within a pre-defined range. This boundedness ensures that the control actions generated by the PPO agent remain within safe operating limits, and thus maintain the stability of the EV system throughout operation.

3.3 Design of PPO-Based ADRC for Electric Vehicle Control

The PPO agent is defined to determine the optimal gains of the ADRC controller by making a scenario that provides this possibility the agent maximizes the reward (reinforcement) signals through interacting with the EV system. The optimal gains designed by the PPO agent are adopted to produce the ADRC command that regulates the speed-tracking problem of the test system. Among the various parameters of the ADRC controller, the gains of NLSEF (β_1 and β_2) play a critical role in regulating the closed-loop problem. Therefore, the actor net produces two separate regulatory signals including agent-1 and agent-2 to adjust the gains of the ADRC controller. To obtain optimal performance of the ADRC controller, the actor and critic nets of the PPO algorithm are trained to adjust the gains of NLSEF as $\beta_1 = \beta_{0,1} + \Delta\beta_1$ and $\beta_2 = \beta_{0,2} + \Delta\beta_2$. Here, $\beta_{0,1}$ and $\beta_{0,2}$ are initial gains of β_1 and β_2, respectively. Terms of $\Delta\beta_1$ and $\Delta\beta_2$ denote ouputs of actions of agent-1 and agent-2, respectively.

The values of speed error $\left(e_w(t) = w_{ref}(t) - w(t)\right)$ and integral of error are selected as the state vector, i.e.,

$$s = \left(e_w(t), \int e_w(t)dt\right) \tag{27}$$

The agent utilizes the return signals of eq. (28) to evaluate the desirability of control actions to track the reference speed signal. Thus, the reward signal for the EV problem is defined by:

$$r_t = \frac{1}{\left|w_{ref}(t) - w(t)\right|} \tag{28}$$

By maximizing the reward signal, the agent reduces the error between the actual values of the speed signal and its reference value.

In this work, the initial gains of NLSEF are set as $\beta_{0,1} = 22$ and $\beta_{0,2} = 38$. In the architecture of PPO, three fully hidden layers (HLs) are considered for both the actor and critic nets while the activation function of these nets is realized by rectified linear unit (ReLU). The mini-batch size of PPO is set to 64 and the value of the discount factor is given as 0.99. The clipping ratio is given as 0.25.

Remark 3: Since the PPO algorithm utilizes a mini-batch scheme, only a limited number of transitions are sampled to train neural networks.

Table 1 Parameters of EV system

Parameters	value	Parameters	value
$R_a + R_f$	0.2 mH	w_{nom}	2800 r/min
$L_a + L_f$	6.008 Ω	m	800 kg
r	0.25 m	A	1.8
J	0.05 kg m^2	ρ	1.25 (kg/m^3)
$\mathcal{L}_a$	1.776	C_d	0.3
V	0–48 V	Θ	0°
i	78 A (250 max)	r	0.25
G	11	B	0.0002 N.M.s
μ_{rr}	0.015	–	–

4 Simulation and Real-Time Verifications

The EV test system shown in Fig. 2 is developed using MATLAB/Simulink to examine the feasibility of the ADRC controller-based PPO tuner mechanism. The code for the training of the actor and critic neural network is in m.file. The corresponding parameters of the EV system are tabulated in Table 1. Three typical scenarios of the EV system are considered to assess the performance of the suggested data drive controller to regulate the speed output. In the first scenario, generic linear changes of speed under the NEDC with a simulation time of 1200 [s] are applied to the EV system. In the next step, the speed is rapidly varied during the simulation time of 1800 [s] to test the feasibility of the suggested scheme in a more severe condition using the FTP-75 test. To analyze the robustness of the suggested ADRC controller-based PPO, an external disturbance is applied to the system at a specific time of the simulation. Moreover, the superiority of the suggested ADRC controller over SMC, pure ADRC, fuzzy PI controller, and PI controller [40] is demonstrated by assessing the transient performance of the EV system's speed output. In the final step, real-time tests were also conducted on the EV system using the Arduino control board to verify the feasibility of the suggested EV control framework in practice. In this setup, the suggested controller was developed in Simulink/MATLAB. The schematic of the real-time platform is depicted in Fig. 6.

4.1 Scenario 1: Set-Point Tracking Under New European Driving Cycle (NEDC)

In the first scenario, the New European Driving Cycle (NEDC) test is applied to the EV system to validate the performance of the suggested ADRC-based PPO algorithm. The NEDC is used as a standardized test process for

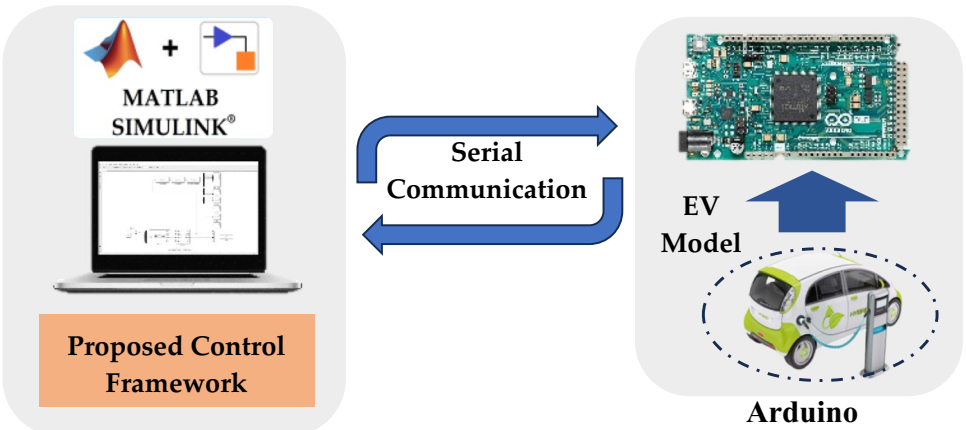

Fig. 6 System configuration for real-time test

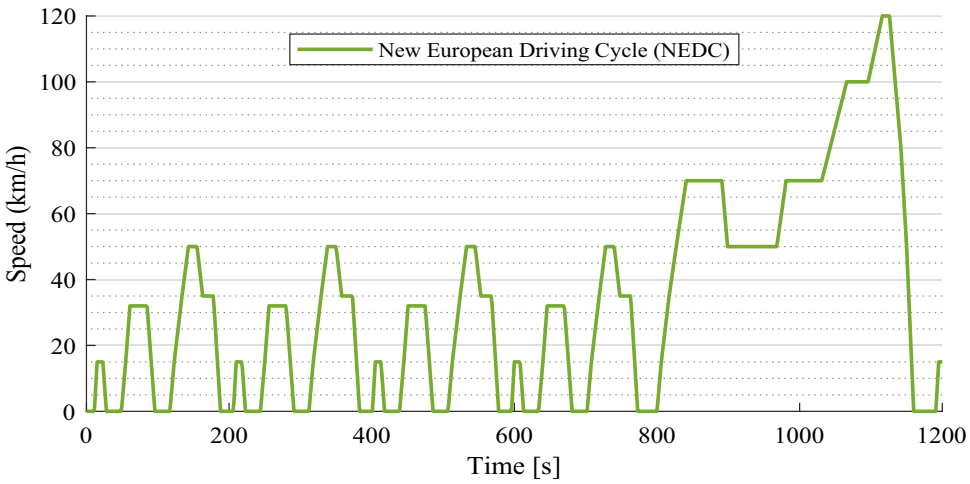

Fig. 7 Graph of New European Driving Cycle (NEDC) test

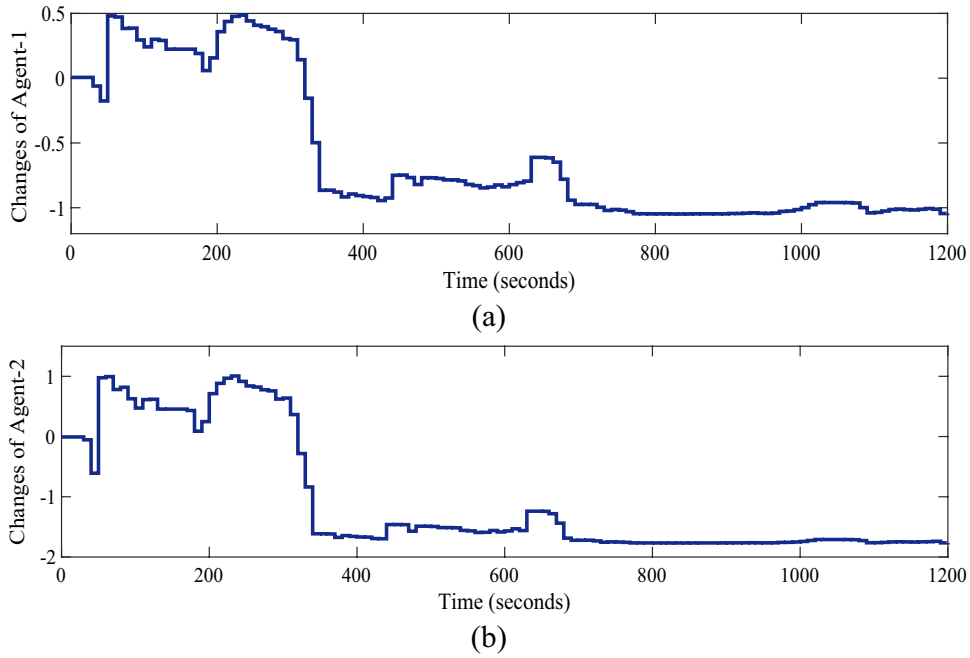

Fig. 8 Curve of changes of PPO's agents

lightweight electric vehicles in Europe to measure the EV system performance under controlled conditions. According to the profile of Fig. 7, the highest speed of NEDC is 120 km per hour.

The curves of changes of agent-1 and agent-2 to regulate the ADRC controller are depicted in Fig. 8a, b, respectively. As depicted in Fig. 8a, b, the values of agent-1 ($\Delta\beta_1$) and agent-2 ($\Delta\beta_2$) are changed during the simulation test. The speed regulation performance of the suggested ADRC controller-based PPO tuner mechanism to track the standardized speed test procedure is depicted in Fig. 9a. For comparative analysis, the outcomes of the SMC, pure ADRC, fuzzy PI controller, and PI controller for the speed tracking problem are also provided in Fig. 9a. As depicted in Fig. 9a, with the application of the suggested ADRC controller (realized by PPO), superior transient performance in terms of settling time and overshoot is achieved in comparison with SMC, pure ADRC, fuzzy PI controller, and PI controller. Moreover, the error signals and armature current produced during the simulation are demonstrated in Fig. 9b, c, respectively. According to these figures, fewer error signals with a lower level of armature current waveforms are generated by utilizing the proposed controller than the two other schemes.

4.2 Scenario 2: Set-Point Tracking under Federal Test Procedure (FTP-75)

In the next step, the FTP-75 test is performed as a reference signal in the simulation to examine the speed regulation capability of the proposed controller under a high level of

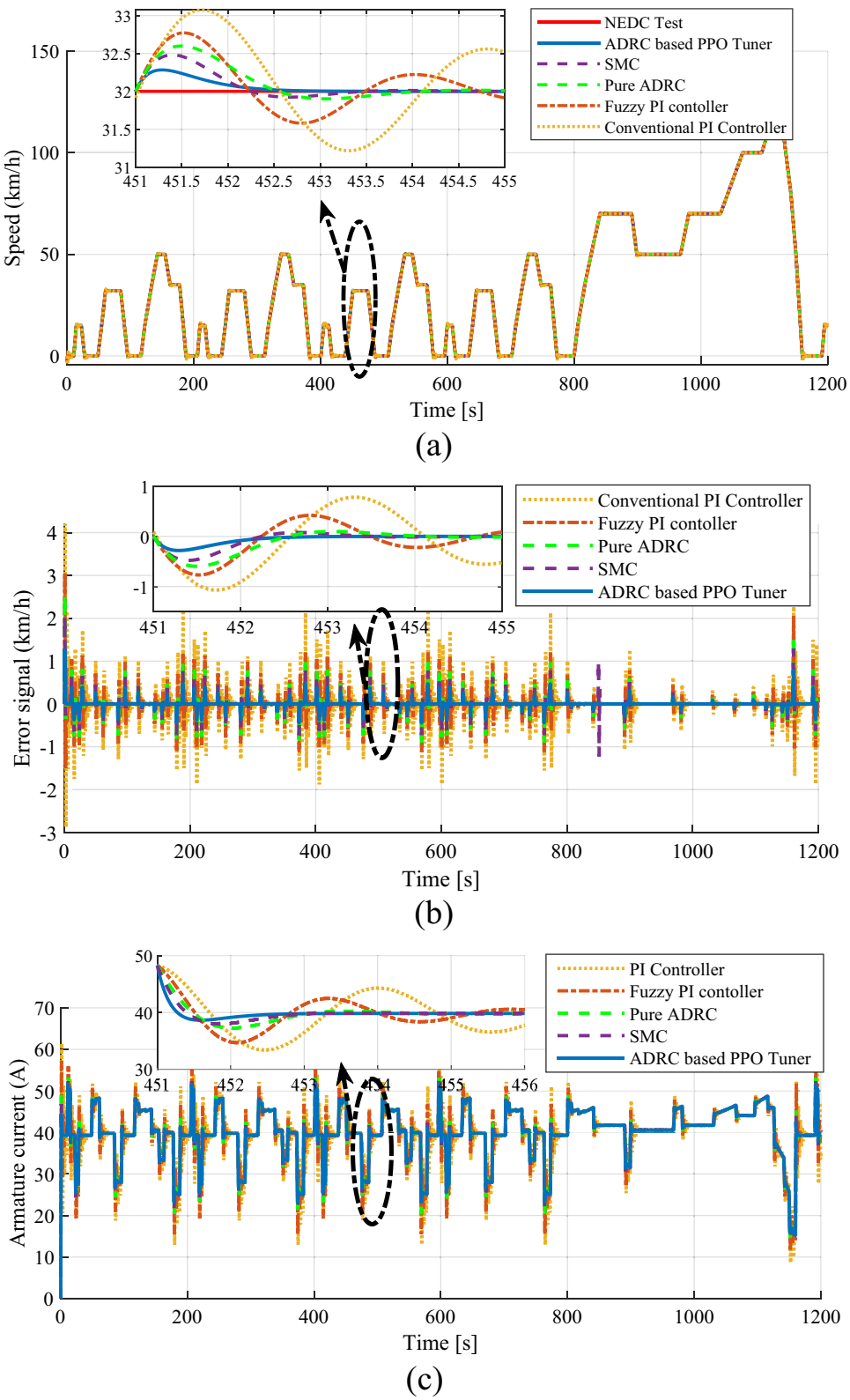

Fig. 9 Performance of ADRC controller (realized by PPO), SMC, pure ADRC, fuzzy PI controller, and PI controller to track NEDC speed examination, **a** speed outcome, **b** error signal, and **c** armature current

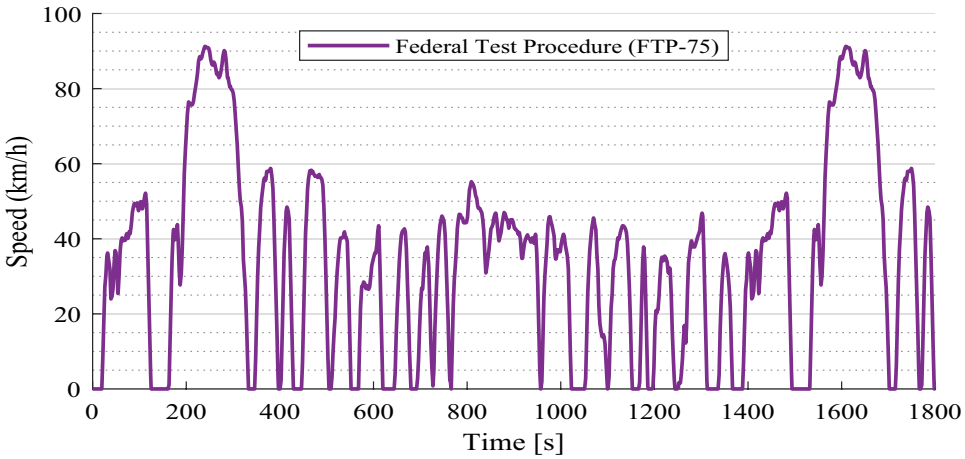

Fig. 10 Graph of Federal Test Procedure (FTP-75) test

speed changes. The profile of FTP-75 is demonstrated in Fig. 10.

The system responses of the EV test system in terms of speed, error signal, and armature current under FTP-75 for various controllers are depicted in Fig. 11. The waveforms in Fig. 11a, b clearly indicate that, when compared to both SMC, pure ADRC, fuzzy PI controller and PI controller, the proposed controller exhibits reduced speed deviation from the reference signal during FTP-75. Additionally, Fig. 11c reveals that the proposed controller generates a lower amount of armature current when the EV system is subjected to the FTP-75 test.

4.3 Scenario 3: Operating Case Under External Disturbance

The disturbance rejection capability of the suggested controller is evaluated in realistic working conditions by imposing a step change to the considered speed tests. An effective and resilient controller should mitigate the effect of disturbance in a short time, ensuring that speed deviation from the reference signal is kept to a minimum. To do this test, a step change with the speed of 1 km/h was applied to NEDC at the 850th second and FTP-75 at the 461th second. The speed outcomes of various controllers under this disturbance are depicted in Fig. 12a, b, respectively. From the sub-figures of Fig. 12, it is demonstrated that the proposed ADRC controller-based PPO tuner can respond to this disturbance more quickly than other control schemes.

To conduct a numerical analysis, the values of the mean square error (MSE), mean absolute error (MAE), and root mean square error (RMSE) for both scenario 1 and scenario 2 are calculated. These performance indices are recognized as crucial metrics for evaluating the accuracy and effectiveness of the system under study. Achieving a minimal speed error is desired, as it reflects the system's capability to optimal outcomes. According to the bar charts of Fig. 13, lower values of error measures in terms of MSE, MAE, and RMSE are obtained by the proposed ADRC-based PPO tuner than other schemes. Specifically, in Scenario 1, the RMSE is 39.83% lower than SMC, 41.22% lower than pure ADRC, 49.02% lower than that of the Fuzzy PI controller, and 66.96% lower than that of the PI controller. In Scenario 2, the improvement percentage over SMC, pure ADRC, Fuzzy PI controller, and PI controller is notably high at 31.03%, 37.18%, 51.09%, and 69.28%, respectively.

4.4 Scenario 4: Robustness Analysis Under Parametric Variations (Real-Time Variation)

In the final step, the dynamic real-time outcomes of EV system under parametric variations are studied. For this purpose, some critical parameters embedded in the EV's model vary depending on their operational condition. In this scenario, the values of $\left(L_a + L_f\right)$, J, μ_{rr}, ρ are varied by 88%, 75%, 85%, and 68%, respectively. Therefore, their values under applied parametric variations are given as 11.30384 Ω for $L_a + L_f$, 0.0875 kg m^2 for J, 0.02775 for μ_{rr}, and 2.1 kg/m^3 for ρ. The speed outcomes under the high level of uncertainties for the NEDC test and FTP-75 test are depicted in Fig. 14a, b. From the real-time responses of Fig. 14, it is confirmed that the suggested EV control provides a lower level of speed fluctuations than other designed controllers.

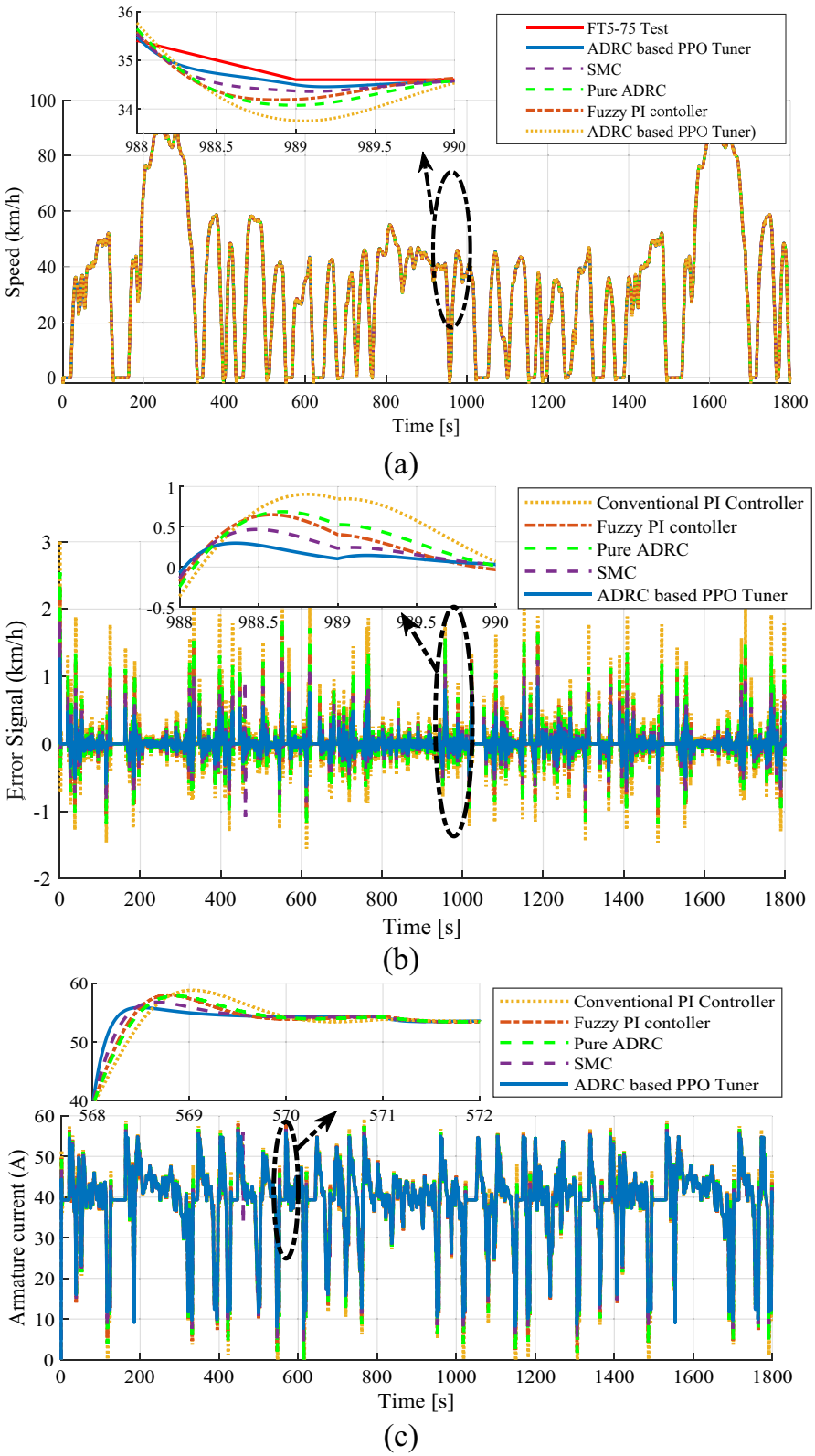

Fig. 11 Performance of ADRC controller (realized by PPO), SMC, pure ADRC, fuzzy PI controller, and PI controller to track FTP-75 speed examination, a) speed outcome, b) error signal, and c) armature current

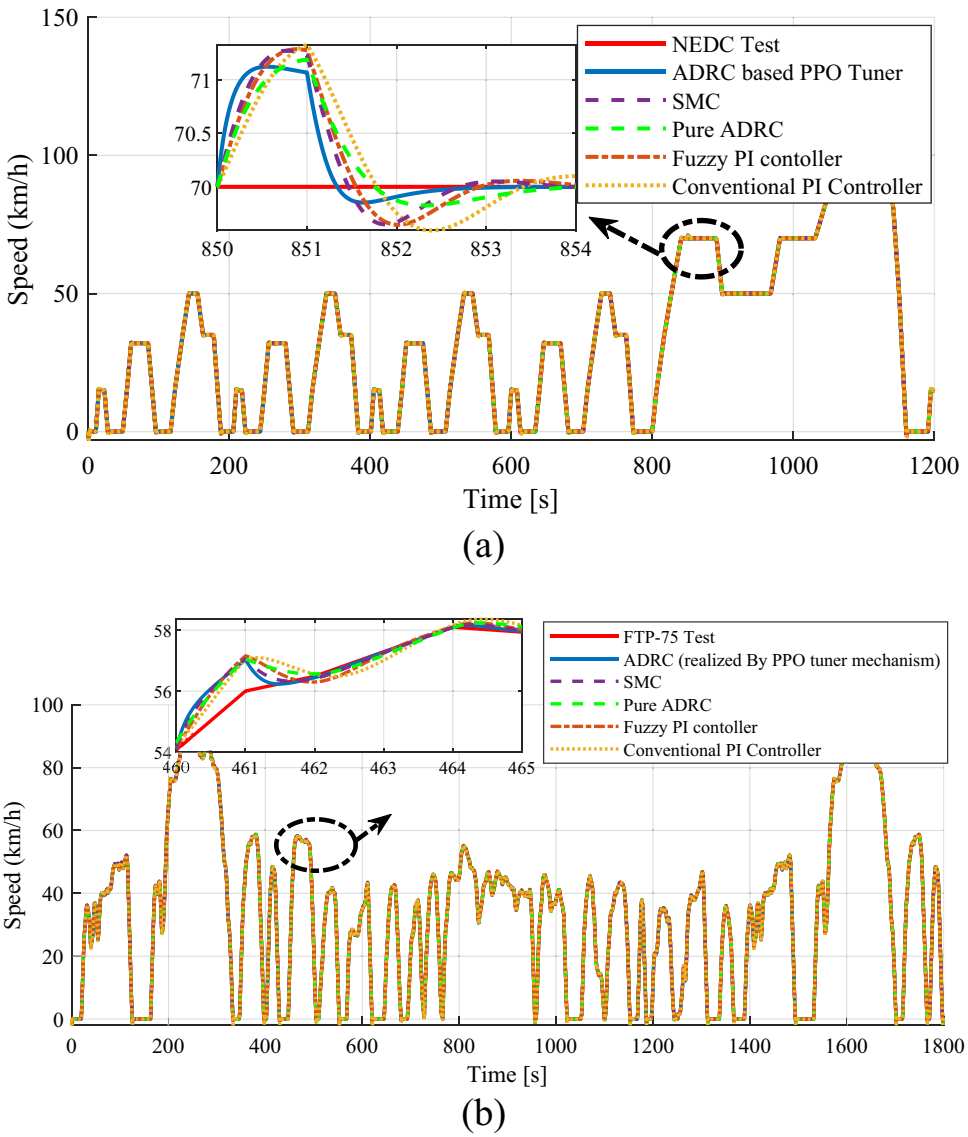

Fig. 12 Performance of designed controllers under external disturbance ADRC controller (realized by PPO), SMC, pure ADRC, fuzzy PI controller, and PI controller, **a** speed outcome of NEDC, and **b** speed outcome of FTP-75

5 Justification of Using the Proposed Framework

While the moded-based controllers rely on the accurate values of system parameters, their sensitivity to uncertainties and un-modeled dynamics degrades the system's performance. To address this issue, a data-driven ADRC controller based on the RL technique has been introduced to regulate the speed of the EV system. By training the PPO during the interaction with the system, the agent aims to learn and optimize the control gains of ADRC, enabling the adaptive ability of the controller to the system uncertainties. Some benefits of the suggested scheme are as follows.

(1) Compared with the model-based schemes, the ADRC controller is applied to the EV system which removes the need to exploit knowledge of the system.
(2) Unlike conventional controllers (e.g., Proportional-Integral (PI) controller, Linear Quadratic Regulator (LQR), etc.) which have limitations to tackle the uncertainties and un-model dynamics, an ESO observer is adopted in the structure of established controller which can estimate all the uncertainties in a straightforward manner.
(3) The training capability of the PPO algorithm is incorporated into the control structure which provides this possibility for the gains of ADRC to adaptively change under both NEDC and FTP-75 driving cycles.

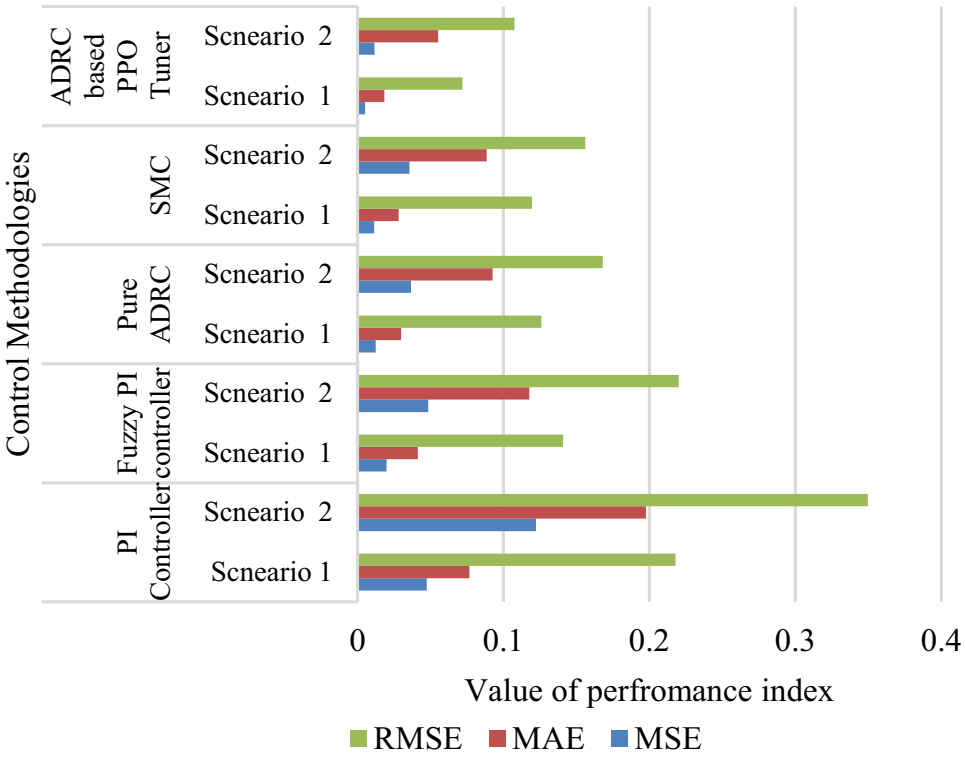

Fig. 13 Comparison of various performance criteria for designed control strategies

(4) The metrics of MSE, MAE, and RMSE validated the superior robustness of the suggested ADRC-based PPO to tackle the NEDC and FTP-75 than SMC, pure ADRC, fuzzy PI controller, and PI controller.
(5) An outstanding feature of the suggested ADRC-based PPO controller in the practical implementation is its adaptability to diverse EV models and real-world driving conditions. This adaptability is validated through comprehensive simulation and real-time test analysis where the suggested controller provided high-level robustness to tackle the EV challenges.

6 Conclusions

In this study, the speed-tracking problem of EV systems has been addressed by designing an adaptive ADRC controller in a data-driven manner. The gains of the NLSEF component in the ADRC controller have been set by the regulatory signals of proximal policy optimization. The two-standardization test profiles including NEDC and FTP-75 tests are applied to the EV system to evaluate the feasibility and usefulness of the suggested controller. The superior transient performance of the ADRC controller (designed by the PPO tuner mechanism) for the speed tracking problem has been compared with SMC, pure ADRC, fuzzy PI controller, and PI controller. The transient outcomes of the EV revealed that the smaller settling time and lesser overshoot are obtained by the suggested controller than the two other control methodologies. The speed stabilization of the test-system is also verified when the EV system is subjected to disturbances. The dynamic responses of speed outcome demonstrated that superior performance of disturbance rejection is achieved by the suggested controller. Furthermore, real-time examinations under parametric variations were conducted to assess the robustness of designed EV's controllers.

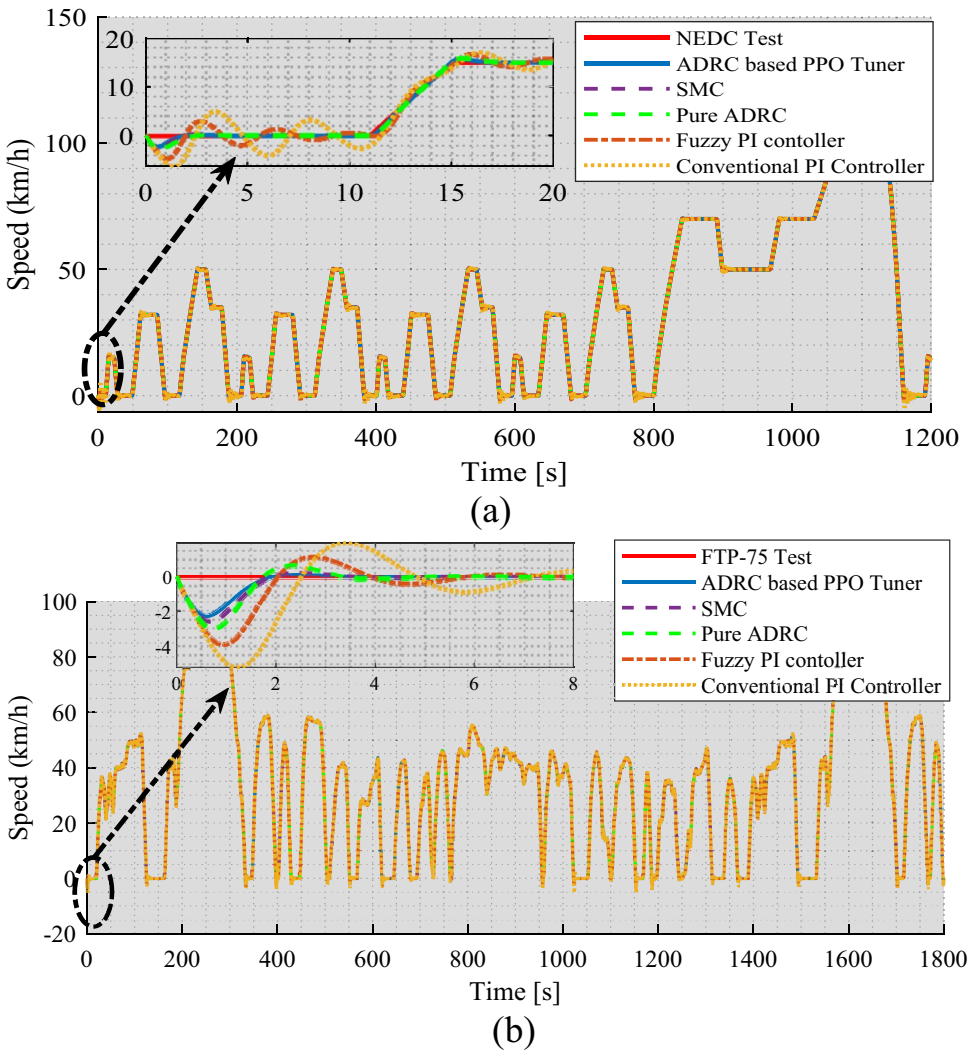

Fig. 14 Rea-Time responses of designed controllers under parametric variations, **a** speed outcome of NEDC, and **b** speed outcome of FTP-75

The future work can be directed toward developing the suggested control framework for various vehicular types such as hybrid electric vehicles (HEVs), plug-in HEVs (PHEVs), and autonomous EVs (AEVs). Examining the scalability of the suggested scheme for various vehicular systems not only is a good option to test its adaptability but also proves its capability for a wide range of transportation systems. The suggested method can be improved using techniques, such as disturbance observers (Zhang et al., 2022), new neural networks (Zhang et al., 2022), and robust controller, such as super-twisting sliding mode control (Lu et al. 2022).

Acknowledgements The authors thank Zhejiang Provincial Department of Education 2023 Annual School-Enterprise Cooperation Project for Domestic Visiting Engineers in Colleges and Universities (FG2023045).

Funding Open access funding provided by Università degli Studi di Roma La Sapienza within the CRUI-CARE Agreement.

Data availability This work has no associated dataset.

References

Ahmed, E. M., Mohamed, E. A., Elmelegi, A., Aly, M., & Elbaksawi, O. (2021). Optimum modified fractional order controller

for future electric vehicles and renewable energy-based interconnected power systems. *IEEE Access, 9*, 29993–30010.

Alrubaie, A. J., Salem, M., Yahya, K., Mohamed, M., & Kamarol, M. (2023). A comprehensive review of electric vehicle charging stations with solar photovoltaic system considering market, technical requirements, network implications, and future challenges. *Sustainability, 15*, 8122.

Bhatti, U. A., Zhaoyuan, Yu., Chanussot, J., Zeeshan, Z., Yuan, L., Luo, W., Nawaz, S. A., Bhatti, M. A., Ain, Q. U., & Mehmood, A. (2021). Local similarity-based spatial–spectral fusion hyperspectral image classification with deep CNN and Gabor filtering. *IEEE Transactions on Geoscience and Remote Sensing, 60*, 1–15.

Bhatti, U. A., Huang, M., Neira-Molina, H., Marjan, S., Baryalai, M., Tang, H., Guilu, Wu., & Bazai, S. U. (2023). MFFCG–multi feature fusion for hyperspectral image classification using graph attention network. *Expert Systems with Applications, 229*, 120496.

Bozhi, M. M., Gilani, V. N. M., Amjad, A., Majid, M. S., Yahya, K., & Salem, M. (2023). A review of wireless pavement system based on the inductive power transfer in electric vehicles. *Sustainability, 15*, 14893.

Bristi, S. D., Tatha, M. J., Ali, M. F., Bhatti, U. A., Sarker, S. K., Masud, M., Ghadi, Y. Y., Algarni, A., & Saha, D. K. (2023). A meta-heuristic sustainable intelligent internet of things framework for bearing fault diagnosis of electric motor under variable load conditions. *Sustainability, 15*, 16722.

Chen, H., Zhang, Yu., Bhatti, U. A., & Huang, M. (2023). Safe decision controller for autonomous drivingbased on deep reinforcement learning in nondeterministic environment. *Sensors, 23*, 1198.

Cheng, S., Li, L., Liu, C.-Z., Xiuheng, Wu., Fang, S.-N., & Yong, J.-W. (2020). Robust LMI-based H-infinite controller integrating AFS and DYC of autonomous vehicles with parametric uncertainties. *IEEE Transactions on Systems, Man, and Cybernetics: Systems, 51*, 6901–6910.

Dabbaghjamanesh, M., Moeini, A., & Kavousi-Fard, A. (2020). Reinforcement learning-based load forecasting of electric vehicle charging station using Q-learning technique. *IEEE Transactions on Industrial Informatics, 17*, 4229–4237.

Das, H. S., Nurunnabi, Md., Salem, M., Li, S., & Rahman, M. M. (2022). Utilization of electric vehicle grid integration system for power grid ancillary services. *Energies, 15*, 8623.

Deng, Z. W., Zhao, Y. Q., Wang, B. H., Gao, W., Xinxin, J., & Kong, M. (2022). A preview driver model based on sliding-mode and fuzzy control for articulated heavy vehicle. *Meccanica, 57*, 1853–1878.

Djouahi, A., Negrou, B., Touggui, Y., & Samy, M. M. (2023). Optimal sizing and thermal control in a fuel cell hybrid electric vehicle via FC-HEV application. *Journal of the Brazilian Society of Mechanical Sciences and Engineering, 45*, 533.

George, M. A., Kamat, D. V., & Kurian, C. P. (2021). Electronically tunable ACO based fuzzy FOPID controller for effective speed control of electric vehicle. *IEEE Access, 9*, 73392–73412.

Haddoun, A., El Hachemi, M., Benbouzid, D. D., Abdessemed, R., Ghouili, J., & Srairi, K. (2008). Modeling, analysis, and neural network control of an EV electrical differential. *IEEE Transactions on Industrial Electronics, 55*, 2286–2294.

Hasan, M. W., Mohammed, A. S., & Noaman, S. F. (2024). An adaptive neuro-fuzzy with nonlinear PID controller design for electric vehicles. *IFAC Journal of Systems and Control, 27*, 100238.

Hu, X., Liu, T., Qi, X., & Barth, M. (2019). Reinforcement learning for hybrid and plug-in hybrid electric vehicle energy management: Recent advances and prospects. *IEEE Industrial Electronics Magazine, 13*, 16–25.

Hwang, F. S., Confrey, T., Reidy, C., Picovici, D., Callaghan, D., Culliton, D., & Nolan, C. (2024). Review of battery thermal management systems in electric vehicles. *Renewable and Sustainable Energy Reviews, 192*, 114171.

Kang, C., Wang, S., Ren, W., Yang, Lu., & Wang, B. (2019). Optimization design and application of active disturbance rejection controller based on intelligent algorithm. *IEEE Access, 7*, 59862–59870.

Khooban, M. H., Niknam, T., Blaabjerg, F., & Dehghani, M. (2016a). Free chattering hybrid sliding mode control for a class of nonlinear systems: Electric vehicles as a case study. *IET Science, Measurement & Technology, 10*, 776–785.

Khooban, M. H., Niknam, T., & Sha-Sadeghi, M. (2016b). Speed control of electrical vehicles: A time-varying proportional–integral controller-based type-2 fuzzy logic. *IET Science, Measurement & Technology, 10*, 185–192.

Li, H., He, Bo., Yin, Q., Xiaokai, Mu., Zhang, J., Wan, J., Wang, D., & Shen, Y. (2019). Fuzzy optimized MFAC based on ADRC in AUV heading control. *Electronics, 8*, 608.

Li, Xiao, Yunkun Shi, and Qi Zhang. 2021. "Cascade PD-ADRC Design for Quadrotor UAV Based on Fractional Order PSO Algorithm." In: *International Conference on Autonomous Unmanned Systems*. Springer, pp. 665–76

Li, Xiaofan, Xiang Luo, and Kunhong Dou. 2022. "Decoupling Control for Hip Joint of Humanoid Robot Based on ADRC." In: *2022 IEEE International Conference on Robotics and Biomimetics (ROBIO)*. IEEE, pp. 2104–09

Liu, X., Fotouhi, A., & Auger, D. (2022). Application of advanced tree search and proximal policy optimization on formula-E race strategy development. *Expert Systems with Applications, 197*, 116718.

Mamo, T., Gopal, R., & Yoseph, B. (2024). Modeling and predesign analysis of electric vehicle considering ethiopian driving cycle. *International Journal of Automotive Technology*. https://doi.org/10.1007/s12239-024-00045-3.

Meng, YiBo., Liu, BingYou, & Wang, LiChao. (2019). Speed control of PMSM based on an optimized ADRC controller. *Mathematical Problems in Engineering, 2019*(2019), 1074702.

Niu, Tao, Hejin Xiong, and Shiqi Zhao. 2016. "Based on ADRC UAV longitudinal pitching Angle control research." In: *2016 IEEE Information Technology, Networking, Electronic and Automation Control Conference*, 21–25. IEEE.

Ozcelik, M. B., Kesici, M., Aksoy, N., & Genc, I. (2022). Reinforcement learning-based demand-side management by smart charging of electric vehicles. *Electrical Engineering, 104*, 3933–3942.

Pang, H., Yao, R., Wang, P., & Zijun, Xu. (2021). Adaptive backstepping robust tracking control for stabilizing lateral dynamics of electric vehicles with uncertain parameters and external disturbances. *Control Engineering Practice, 110*, 104781.

Pazouki, S., & Olamaei, J. (2019). The effect of heterogeneous electric vehicles with different battery capacities in parking lots on peak load of electric power distribution networks. *International Journal of Ambient Energy, 40*, 734–738.

Qiu, D., Wang, Yi., Hua, W., & Strbac, G. (2023). Reinforcement learning for electric vehicle applications in power systems: A critical review. *Renewable and Sustainable Energy Reviews, 173*, 113052.

Ristiana, R., Rohman, A. S., Machbub, C., Purwadi, A., & Rijanto, E. (2019). A new approach of EV modeling and its control applications to reduce energy consumption. *IEEE Access, 7*, 141209–141225.

Shiyong, W., Khan, A., Lin, Y., Jiang, Z., Tang, H., Alomar, S. Y., Sanaullah, M., & Bhatti, U. A. (2023). Deep reinforcement learning enables adaptive-image augmentation for automated optical inspection of plant rust. *Frontiers in Plant Science, 14*, 1142957.

Subroto, R. K., Wang, C. Z., & Lian, K. L. (2020). Four-wheel independent drive electric vehicle stability control using novel adaptive sliding mode control. *IEEE Transactions on Industry Applications, 56*, 5995–6006.

Tao, L., Chen, Q., Nan, Y., Dong, F., & Jin, Y. (2018). Speed tracking and synchronization of a multimotor system based on fuzzy ADRC and enhanced adjacent coupling scheme. *Complexity, 2018*(2018), 5632939.

Tao, L., Wang, P., Wang, Y., Ma, X., Cheng, P., & Zhao, D. (2021). Variable structure ADRC-based control for load-side buck interface converter: Formation, analysis, and verification. *IEEE Transactions on Industrial Electronics, 69*, 6236–6246.

Veysi, M., Aghaei, J., Shasadeghi, M., Razzaghi, R., Bahrani, B., & Ryan, D. J. (2020). Energy-efficient speed control of electric vehicles: Linear matrix inequality approach. *IEEE Transactions on Vehicular Technology, 69*, 10469–10483.

Wu, Z., Li, D., Xue, Y., & Chen, YangQuan. (2019). Gain scheduling design based on active disturbance rejection control for thermal power plant under full operating conditions. *Energy, 185*, 744–762.

Wu, A., Mao, J.-F., & Zhang, X. (2020). An ADRC-based hardware-in-the-loop system for maximum power point tracking of a wind power generation system. *IEEE Access, 8*, 226119–226130.

Xia, Anjun, Xu Li, Shuju Hu, Nianhong Li, and Honghua Xu. 2013. "A new pitch control method for large scale wind turbine based on ADRC." In *2013 International Conference on Materials for Renewable Energy and Environment*. IEEE, pp. 373–76

Xiao, Zhu, Jinmei Shu, Hongbo Jiang, Geyong Min, Jinwen Liang, Arun J, IEEE Transactions on Mobile Computing Iyengar. 2023. 'Toward collaborative occlusion-free perception in connected autonomous vehicles'.

Yang, X., Huang, Qi., Jing, S., Zhang, M., Zuo, Z., & Wang, S. (2022). Servo system control of satcom on the move based on improved ADRC controller. *Energy Reports, 8*, 1062–1070.

Yingtao, Lu., Tan, C., Ge, W., Zhao, Y., Smart, G. J., & Wang, M. (2022). Adaptive disturbance observer-based improved super-twisting sliding mode control for electromagnetic direct-drive pump. *Smart Materials and Structures, 32*, 017001.

Zhang, X., Wang, Y., Yuan, X., Shen, Y., & Zhangyu, Lu. (2022). Adaptive dynamic surface control with disturbance observers for battery/supercapacitor-based hybrid energy sources in electric vehicles. *J IEEE Transactions on Transportation Electrification, 9*, 5165–5181.

Zhang, H., Zhou, C., Wang, C., & Zhao, W. (2023). An energy efficient control strategy for electric vehicle driven by in-wheel-motors based on discrete adaptive sliding mode control. *Chinese Journal of Mechanical Engineering, 36*, 58.

Zhang Xiaoliang, Xia Jiang, Nan Li, Zhongyue Yang, Zhuang Xiong, and Jian Zhang. 2021. "Eco-driving for intelligent electric vehicles at signalized intersection: A proximal policy optimization approach." In: *ISCTT 2021; 6th International Conference on Information Science, Computer Technology and Transportation*, VDE, 1–7.

Zhao, Y., & Dong, L. (2019). Robust current and speed control of a permanent magnet synchronous motor using SMC and ADRC. *Control Theory and Technology, 17*, 190–199.

Zhu, B., Huang, Y., Fan, L., Ma, Y., Wang, B., Xia, C., Afzal, M., Zhang, B., Dong, W., & Wang, H. (2016). Novel fuel cell with nanocomposite functional layer designed by perovskite solar cell principle. *Nano Energy, 19*, 156–164.